Unconventional Spin Relaxation Involving Localized Vibrational Modes in Ho Single-Atom Magnets

F. Donati,[1,2,3] S. Rusponi,[2] S. Stepanow,[4] L. Persichetti,[4,5] A. Singha,[1,2,3] D. M. Juraschek,[4,6]
C. Wäckerlin,[2,7] R. Baltic,[2] M. Pivetta,[2] K. Diller,[2] C. Nistor,[4] J. Dreiser,[8] K. Kummer,[9] E. Velez-Fort,[9]
N. A. Spaldin,[4] H. Brune,[2] and P. Gambardella[4]

[1]Center for Quantum Nanoscience, Institute for Basic Science (IBS), 03760 Seoul, Republic of Korea
[2]Institute of Physics, École Polytechnique Fédérale de Lausanne (EPFL), Station 3, CH-1015 Lausanne, Switzerland
[3]Department of Physics, Ewha Womans University, Seoul 03760, Republic of Korea
[4]Department of Materials, ETH Zurich, Hönggerbergring 64, CH-8093 Zurich, Switzerland
[5]Department of Sciences, Roma Tre University, I-00146, Roma, Italy
[6]Harvard John A. Paulson School of Engineering and Applied Sciences, Harvard University, Cambridge, Massachusetts 02138, USA
[7]Institute of Physics of the Czech Academy of Sciences, Cukrovarnická 10, 16200 Prague 6, Czech Republic
[8]Swiss Light Source (SLS), Paul Scherrer Institute (PSI), CH-5232 Villigen PSI, Switzerland
[9]European Synchrotron Radiation Facility (ESRF), F-38043 Grenoble, France

We investigate the spin relaxation of Ho single atom magnets on MgO/Ag(100) as a function of temperature and magnetic field. We find that the spin relaxation is thermally activated at low field, while it remains larger than 1000 s up to 30 K and 8 T. This behavior contrasts with that of single molecule magnets and bulk paramagnetic impurities, which relax faster at high field. Combining our results with density functional theory, we rationalize this unconventional behavior by showing that local vibrations activate a two-phonon Raman process with a relaxation rate that peaks near zero field and is suppressed at high field. Our work shows the importance of these excitations in the relaxation of axially coordinated magnetic atoms.

The exploration of magnetic atomic-scale units for logical operations [1] and data storage [2] has revived interest in the spin relaxation mechanisms of systems composed of one or few magnetic atoms in a nonmagnetic environment. Early studies on polymetallic [3,4] and single ion molecular magnets (SIMMs) [5–7] showed that the spin relaxation below 4 K can be sufficiently slow to enable the observation of magnetic hysteresis [8,9]. Effective strategies employed to increase the spin relaxation time, hence the temperature range of magnetic bistability, rely on engineering the ligand field so as to maximize the uniaxial magnetic anisotropy and, consequently, the effective barrier for magnetization reversal U_{eff} [10–12]. Recently, it has been shown that the hysteretic behavior can be reinforced by minimizing underbarrier relaxation pathways and engineering the coupling between the vibrational modes of the ligands and the magnetic states of the core [13–15]. Combining these approaches has enabled hysteresis up to unprecedented temperatures of 72 [16] and 80 K [17].

Individual magnetic atoms adsorbed on a single crystal surface allow for exploring magnetic anisotropy [18–21] and bistability [22–24] in a simplified ligand environment. In such a configuration, one can achieve maximal uniaxial anisotropy and minimal coordination of the magnetic atoms [21,22,25,26]. As will be shown here, the latter has the

additional effect of reducing the coupling of the spin to the phonon modes of the substrate. The validity of this approach was demonstrated by the observation of magnetic remanence up to 40 K in Ho atoms on MgO/Ag(100), first with x-ray absorption spectroscopy (XAS) and magnetic circular dichroism (XMCD) [22], and subsequently confirmed by scanning tunneling microscopy (STM) [24,27]. These single-bond-coordinated atom magnets are ideal systems for investigating the fundamental mechanisms causing magnetization reversal. Addressing these mechanisms requires measuring the lifetime of the magnetic states as a function of temperature and magnetic field. For systems with very long lifetimes, these measurements can be performed with accurate statistics using ensemble-averaging techniques.

Here, we combine XAS and XMCD experiments with density functional theory (DFT) to shed light on the magnetic reversal of Ho atoms on MgO/Ag(100). By recording the time evolution of the XMCD intensity, we directly access the magnetic lifetime τ as a function of temperature T and external magnetic field B. At $B = 0.01$ T, the Ho atoms show $\tau \approx 1500$ s up to 10 K, and an exponential decrease of τ with T down to about 100 s at 30 K. Remarkably, we observe that the lifetime measured at $B = 6.8$ T does not show any significant variation with temperature, and remains constant
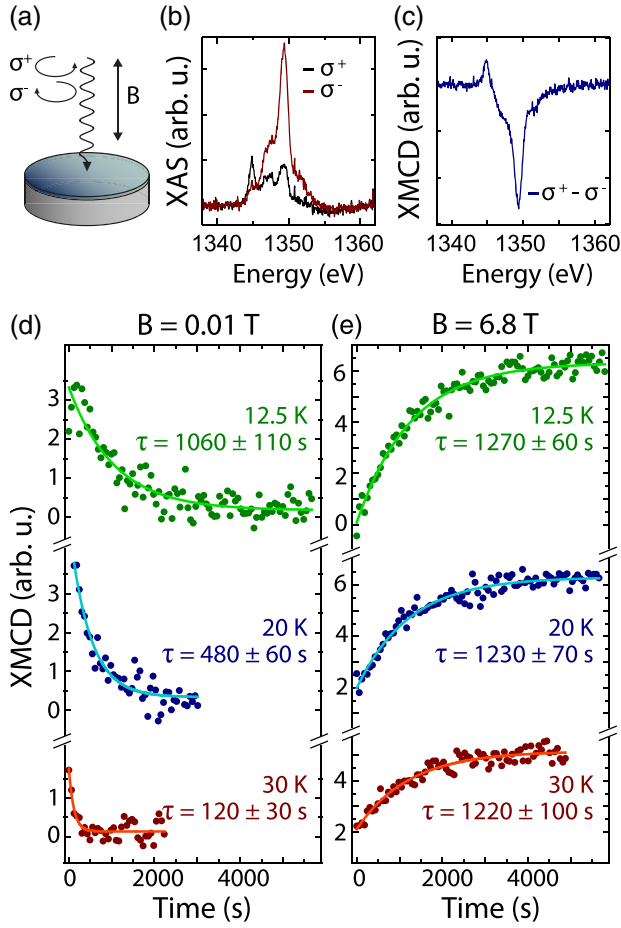
FIG. 1. (a) Sketch of the measurement geometry. (b) XAS and (c) XMCD of the Ho atoms on MgO/Ag(100) at the M_5 edge ($B = 6.8$ T, $T = 2.5$ K, Ho coverage $\Theta_{Ho} \approx 0.015$ ML). (d) Time evolution of the peak XMCD intensity at $B = 0.01$ T after saturating the ensemble at $+6.8$ T, and (e) at $B = +6.8$ T after saturating the ensemble at -6.8 T.

at about 1200 s up to 30 K. Field-dependent characterization of the magnetic lifetime indicates that suppression of the reversal mechanism occurs above $B = 0.3$ T. We use DFT to show that only local vibrational modes of the Ho atoms allow for an efficient exchange of energy and momentum between the spin and phonon reservoirs. We propose that this frustrated exchange of energy is responsible for the extremely long magnetic lifetimes of Ho atoms.

The XAS and XMCD measurements were performed at the EPFL/PSI X-Treme beam line of the Swiss Light Source [28] and at the ID32 beam line of the European Synchrotron Radiation Facility [29]. All the measurements were performed in normal incidence geometry with circularly polarized light in total electron yield mode with the external magnetic field parallel to the x-ray beam, see Fig. 1(a) [30]. The magnetic lifetime of the ensemble of Ho atoms was obtained by recording the evolution of the XMCD signal both at low ($B = 0.01$ T) and high fields (up to $B = 8$ T) after having stabilized the sample temperature

at the desired value. The low field measurements were performed by (i) saturating the ensemble at the largest positive magnetic field, (ii) sweeping the field to $B = +0.01$ T at the maximum rate of 33 mT/s, and (iii) acquiring the XAS signal for the two circular polarizations at the maximum of the Ho M_5 absorption edge as a function of time [30]. High-field measurements were recorded following a similar procedure after saturating the ensemble at the largest negative field.

Figure 1(b) shows the XAS spectra acquired at the Ho M_5 edge for the two circular polarizations. The difference gives the XMCD shown in Fig. 1(c). Ho atoms on MgO/Ag(100) present a strong out-of-plane magnetic anisotropy, with the ground state being a magnetic doublet [22,24] separated by a few tens of meV from the first excited states [27]. For such an Ising-like system, the intensity of the XMCD peak reflects the average occupation of the lowest magnetic doublet. Therefore, the time evolution of the peak provides the lifetime of the magnetic states [22,23,31].

Figure 1(d) shows the evolution of the XMCD intensity at low magnetic field and three different temperatures. The data fit well to a single exponential function with vanishing asymptotic magnetization, yielding the characteristic lifetime τ of the Ho atoms. For increasing temperatures, we observe a decrease of the lifetime from 1060 ± 110 s at 12.5 K to 120 ± 30 s at 30 K. For bulk paramagnetic impurities [32,33] and molecular magnets [3–6,10–12,34], the well-known reduction of the magnetic lifetime with increasing temperature is attributed to spin-phonon scattering. These mechanisms become increasingly efficient as the number of phonons available for the absorption processes increases with temperature [35]. Figure 1(e) shows the evolution of the XMCD of Ho atoms recorded at $B = 6.8$ T. Also in this case, we observe an exponential time dependence of the XMCD. The positive asymptotic value reflects the intensity of the dichroism at the maximum available field, which decreases with the sample temperature. However, differently from the low field case, τ is here unaffected by temperature and remains constant at a value of about 1200 s.

Figure 2 shows τ as a function of temperature measured at low and high fields. Below 10 K, the relaxation rate is dominated by the scattering with the secondary electrons generated in the x-ray absorption process [22,31,36]. These hot electrons represent a temperature-independent extrinsic source of magnetic relaxation that can only be minimized by reducing the photon flux while still having a sufficient x-ray absorption signal. Above 10 K, τ behaves very differently depending on the applied field. At $B = 0.01$ T, τ follows an exponential behavior typical of an activated process up to the maximum measured temperature of 30 K. At $B = 6.8$ T, τ remains constant and independent of temperature. This behavior is very different from that of other SIMMs [6,10–12,31,37] and single atom magnets [23], which all show increased spin relaxation at high field.
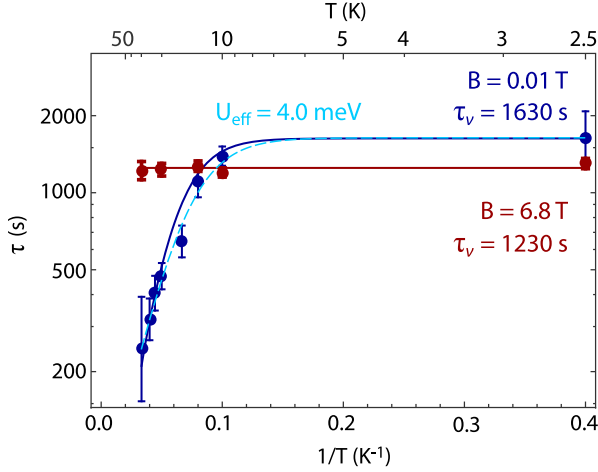
FIG. 2. Magnetic lifetime τ versus temperature for $B = 0.01$ (blue dots) and $B = 6.8$ T (red dots). The cyan dashed line is a fit with Eq. (1). Blue and red solid lines are fits to the low and high field data, respectively, using the two-phonon model described in the text.

The temperature dependence of τ at $B = 0.01$ T can be fit by

$$\tau^{-1} = \tau_\nu^{-1} + [\tau_0 \exp(U_{\text{eff}}/k_B T)]^{-1}, \qquad (1)$$

where $\tau_\nu = 1630$ s is the photon-limited lifetime due to the secondary electrons [22] and the exponential term describes a thermally activated relaxation with an effective barrier $U_{\text{eff}} = 4 \pm 1$ meV and a prefactor $\tau_0 = 60 \pm 30$ s [30]. Such an exponential temperature behavior is conventionally associated with a two-phonon Orbach process involving an excited spin state, whose separation from the ground state defines the activation barrier [35]. However, typical prefactors for the Orbach process range from 10^{-6} to 10^{-11} s [6,8,14,32,38], which are orders of magnitude smaller than the τ_0 estimated for Ho. Additionally, STM experiments show that the excited states lie at least 15 meV above the ground state doublet [24,27], which is not compatible with the barrier derived from the fit. In fact, even qualitatively, the suppression of spin reversal at high fields is neither compatible with a conventional Orbach mechanism, which predicts an increase of the relaxation rate due to the Zeeman shift of the levels defining the activation barrier, nor with a Raman process activated by delocalized substrate phonons, whose relaxation rate also increases with increasing Zeeman splitting of the lowest doublet [30].

To obtain further insight into the field dependence, we measure the magnetic lifetime of Ho atoms at two selected temperatures, 2.5 and 22 K, as a function of magnetic field. As shown in Fig. 3, at 2.5 K, τ is constant within the error bars, remaining well above 1000 s up to 7 T. On the other hand, at 22 K, τ decreases strongly below 0.3 T, see inset, whereas no clear trend is visible at higher field [39].
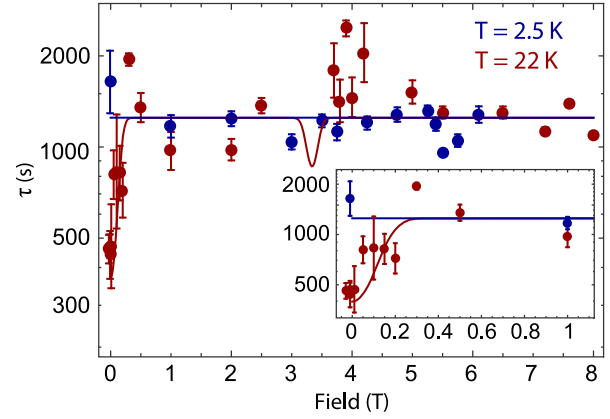
FIG. 3. Magnetic lifetime τ versus magnetic field measured at 2.5 (blue dots) and 22 K (red dots). Blue and red solid lines are fits using the two-phonon model described in the text. Inset: magnification of the field range below $B = 1$ T.

In contrast with this behavior, a faster magnetic relaxation at high field is typically observed in SIMMs, which is ascribed to the direct transition between the two states of the lowest spin doublet mediated by the emission or absorption of a phonon. As the splitting of the magnetic levels increases with the applied field, more phonon states become available for these transitions, hence their relaxation rate increases as well [35]. For Ho single atom magnets, the absence of temperature- and field-dependent relaxation from 0.3 to 8 T indicates that the direct relaxation process is slower than the photon-induced relaxation up to the longest timescale available in our experiments (thousands of seconds).

The magnetic lifetime of Ho atoms on MgO/Ag(100) is thus not compatible with conventional models of spin relaxation based on either direct, Orbach, or Raman processes, as none of these models can explain an activated process that takes place exclusively at low field. A common feature of these models is that the phonon density of states (DOS) is assumed to be a continuum. This assumption is questionable in the case of adatoms, for which strong resonances are expected in correspondence of the local vibrational modes of the atom-surface complex. DFT calculations of a Ho atom adsorbed on a slab of 3 monolayers (ML) of MgO [30] provide insight into the vibrational structure of our system. Figure 4(a) shows the calculated phonon DOS projected onto the Ho atom and the MgO slab, respectively, for a Ho atom adsorbed on top of a surface oxygen ion [22,26]. The MgO phonon DOS shows a linear behavior owing to the two-dimensional phonon dispersion of the ultrathin slab. The Ho phonon DOS, on the other hand, presents two strong resonances corresponding to a doubly degenerate in-plane Ho-O vibration with an energy at the Brillouin zone center of $E_\parallel = 4.7$ meV and an out-of-plane Ho-O vibration with an energy of $E_\perp = 8.6$ meV. In the C_{4v} symmetry of the adsorption site, the two in-plane modes are degenerate, see
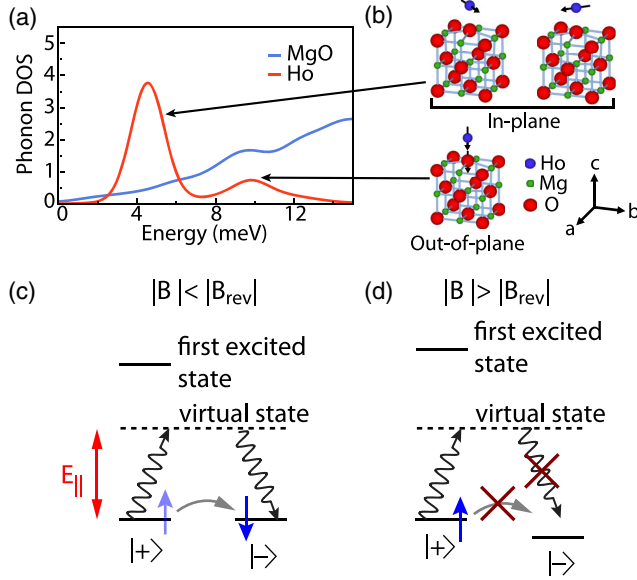
FIG. 4. (a) Calculated low-energy phonon DOS projected onto the Ho atom and MgO slab (see Ref. [30] for the full range plot). (b) Eigenvector of the modes with large displacement of the Ho atoms. (c) Schematics of the two-phonon process responsible for the thermally activated relaxation at low field and high temperature. (d) In high field, this mechanism is suppressed due to the energy mismatch of the lowest states.

Fig. 4(b). Remarkably, the energy of the in-plane modes matches the activation barrier U_{eff} inferred from our measurements.

Motivated by these observations, we surmise that the peculiar magnetic behavior of Ho single atom magnets is influenced by the contribution of local vibrational modes to the spin-phonon coupling [15,40]. The relaxation process is thermally activated and occurs only at low magnetic fields, i.e., when the two spin levels of the lowest doublet are very close in energy. Further, the exceedingly long τ_0 suggests that relaxation occurs via a higher order process involving the simultaneous absorption and emission of more than one phonon. Based on these assumptions, we develop a model based on the coupling of a single spin to local vibration modes via a two-phonon Raman process [41]. Since the relaxation due to quantum tunneling of the magnetization and direct processes is slower than that induced by photon absorption, these processes are not included in the model. The spin reversal from $|+\rangle$ to $|-\rangle$ and back occurs at a rate $\tau_s(B,T)^{-1} = \Gamma(B,T)[1 + \exp(-\Delta/k_B T)]$, with the transition probability obtained from the two-phonon integral [35,41]

$$\Gamma(B,T) = \kappa \int \rho_{\text{Ho}}(\omega,T) \rho_{\text{Ho}}\left(\omega + \frac{\Delta}{\hbar}, T\right) \exp\frac{\hbar\omega + \Delta}{k_B T} d\omega. \tag{2}$$

Here, ω and $\omega + (\Delta/\hbar)$ are the frequencies of the two phonons involved in the transition, $\Delta = 2\mu_{\text{Ho}}B$ is the

splitting between the two lowest states with $\mu_{\text{Ho}} = 10.1\mu_B$ [24], and κ is the scaling factor that is taken as a free parameter of the model [30]. The phonon energy density

$$\rho_{\text{Ho}}(\omega,T) = D_{\text{Ho}}(\omega)\hbar\omega\left[\exp\left(\frac{\hbar\omega}{k_B T}\right) - 1\right]^{-1} \tag{3}$$

only includes the DOS of the local modes with finite projected displacement of the Ho atoms, $D_{\text{Ho}}(\omega)$ [red line in Fig. 4(a)]. In the model, this term is implemented by summing two Gaussian peaks with energy and relative amplitude as found in DFT [30], while their width ΔE is left as a free parameter. Finally, we calculate $\tau(B,T)$ by adding the photon-limited lifetime τ_ν as in Eq. (1).

As seen from the full curves in Figs. 2 and 3, our model fully reproduces the temperature- and field-dependent data with $\kappa = 1.7 \times 10^{-17}$ and $\Delta E = 0.17$ meV. Although we cannot exclude the contribution of other relaxation processes in the high field region dominated by photon-induced relaxation, we remark that such an agreement cannot be achieved if the delocalized acoustic phonon modes from the MgO substrate were to contribute significantly to the spin relaxation [30]. Therefore, only the modes at $E_\parallel = 4.7$ meV with a large amplitude on the Ho atoms effectively enable the magnetic reversal. The rationale of the reversal mechanism is sketched in Figs. 4(c) and 4(d). For $B < B_{\text{rev}}$, where $B_{\text{rev}} = \Delta E/2\mu_{\text{Ho}}$ is the field required to suppress the reversal, the ground state doublet is close to degeneracy and the two magnetic states can be connected by two local vibrations within their energy broadening ΔE when sufficient thermal energy is provided. Because of the lower activation energy, the relaxation essentially occurs via the in-plane mode. The specific relaxation path involving a low energy local vibrational mode strongly reduces the effective barrier with respect to the zero-field level splitting, i.e., $U_{\text{eff}} = E_\parallel$. A similar barrier reduction was also observed for Fe-based SIMM, but attributed to anharmonic phonons in resonant coupling with excited spin states [13]. Moreover, applying a large magnetic field lifts the degeneracy of the two states such that the same quantum of energy absorbed from one state cannot be reemitted to reach the opposite spin state. In this case, the relaxation process is suppressed. The suppression of this process with external field has, to our knowledge, not been reported so far. The model additionally predicts relaxation by a two phonon process involving an in-plane and an out-of-plane mode, with the difference in energy matching the Zeeman spitting at 3.7 T. The related dip predicted in the curve at high temperature of Fig. 3 is, however, too shallow to be detected with sufficient significance [42].

The linewidth of the spin-flip transition is broadened by the finite lifetime of the vibrational mode [41] as well as by the spread in energy of the Ho nuclear states due to the hyperfine interaction [33,43,44]. By modeling the low-field

and high-temperature data of Fig. 3, we infer that $\Delta E = 0.17 \pm 0.07$ meV. This value essentially coincides within the error bars with the expected hyperfine splitting of Ho atoms [33,43,45], suggesting that this contribution dominates over finite lifetime broadening of the vibrational mode.

In conclusion, single atom magnets at surfaces provide an ideal test for models of spin-lattice relaxation in the presence of strongly localized vibrational modes. Our work shows that, for a single spin system, the presence of local vibrational modes leads to a peak in the Raman relaxation rates near zero field, which is suppressed at high field. For axially coordinated Ho single atom magnets on MgO, we identified the relevant thermal relaxation mechanism as a two-phonon Raman process involving the in-plane displacement of the Ho atom with respect to the O adsorption site. Such an unconventional spin relaxation mechanism might be relevant also in single molecule magnets with a phonon density of states dominated by localized vibrational resonances.

[1] A. A. Khajetoorians, J. Wiebe, B. Chilian, and R. Wiesendanger, Science 332, 1062 (2011).

[2] S. Loth, S. Baumann, C. P. Lutz, D. M. Eigler, and A. J. Heinrich, Science 335, 196 (2012).

[3] R. Sessoli, D. Gatteschi, A. Caneschi, and M. A. Novak, Nature (London) 365, 141 (1993).

[4] M. Mannini, F. Pineider, C. Danieli, L. Totti, F. Sorace, P. Sainctavit, M.-A. Arrio, E. Otero, L. Joly, J. C. Cezar, A. Cornia, and R. Sessoli, Nature (London) 468, 417 (2010).

[5] N. Ishikawa, M. Sugita, T. Ishikawa, S.-y. Koshihara, and Y. Kaizu, J. Am. Chem. Soc. 125, 8694 (2003).

[6] R. Westerström, J. Dreiser, C. Piamonteze, M. Muntwiler, S. Weyeneth, H. Brune, S. Rusponi, F. Nolting, A. Popov, S. Yang, L. Dunsch, and T. Greber, J. Am. Chem. Soc. 134, 9840 (2012).

[7] J. M. Zadrozny, D. J. Xia, M. Atanasov, G. J. Long, F. Grandjean, F. Neese, and J. R. Long, Nat. Chem. 5, 577 (2013).

[8] D. Gatteschi, R. Sessoli, and J. Villain, Molecular Nanomagnets (Oxford University Press, Oxford, 2006).

[9] J. Bartolomé, F. Luis, and J. F. Fernández, Molecular Magnets (Springer, Berlin, 2014).

[10] L. Ungur, J. J. Le Roy, I. Korobkov, M. Murugesu, and L. F. Chibotaru, Angew. Chem. Int. Ed. 53, 4413 (2014).

[11] F. Pointillart, K. Bernot, S. Golhen, B. Le Guennic, T. Guizouarn, L. Ouahab, and O. Cador, Angew. Chem. Int. Ed. 54, 1504 (2015).

[12] Y.-C. Chen, J.-L. Liu, L. Ungur, J. Liu, Q.-W. Li, L.-F. Wang, Z.-P. Ni, L. F. Chibotaru, X.-M. Chen, and M.-L. Tong, J. Am. Chem. Soc. 138, 2829 (2016).

[13] A. Lunghi, F. Totti, R. Sessoli, and S. Sanvito, Nat. Commun. 8, 14620 (2017).

[14] C. A. P. Goodwin, F. Ortu, D. Reta, N. F. Chilton, and D. P. Mills, Nature (London) 548, 439 (2017).

[15] L. Escalera-Moreno, J. J. Baldoví, A. Gaita-Ariño, and E. Coronado, Chem. Sci. 9, 3265 (2018).

[16] K. R. McClain, C. A. Gould, K. Chakarawet, S. J. Teat, T. J. Groshens, J. R. Long, and B. G. Harvey, Chem. Sci. 9, 8492 (2018).

[17] F.-S. Guo, B. M. Day, Y.-C. Chen, M.-L. Tong, A. Mansikkamaki, and R. A. Layfield, Science 362, 1400 (2018).

[18] P. Gambardella, S. Rusponi, M. Veronese, S. S. Dhesi, C. Grazioli, A. Dallmeyer, I. Cabria, R. Zeller, P. H. Dederichs, K. Kern, C. Carbone, and H. Brune, Science 300, 1130 (2003).

[19] C. F. Hirjibehedin, C.-Y. Lin, A. F. Otte, M. Ternes, C. P. Lutz, B. A. Jones, and A. J. Heinrich, Science 317, 1199 (2007).

[20] B. Bryant, A. Spinelli, J. J. T. Wagenaar, M. Gerrits, and A. F. Otte, Phys. Rev. Lett. 111, 127203 (2013).

[21] I. G. Rau, S. Baumann, S. Rusponi, F. Donati, S. Stepanow, L. Gragnaniello, J. Dreiser, C. Piamonteze, F. Nolting, S. Gangopadhyay, O. R. Albertini, R. M. Macfarlane, C. P. Lutz, B. A. Jones, P. Gambardella, A. J. Heinrich, and H. Brune, Science 344, 988 (2014).

[22] F. Donati, S. Rusponi, S. Stepanow, C. Wäckerlin, A. Singha, L. Persichetti, R. Baltic, K. Diller, F. Patthey, E. Fernandes, J. Dreiser, Ž. Šljivančanin, K. Kummer, C. Nistor, P. Gambardella, and H. Brune, Science 352, 318 (2016).

[23] R. Baltic, M. Pivetta, F. Donati, C. Wäckerlin, A. Singha, J. Dreiser, S. Rusponi, and H. Brune, Nano Lett. 16, 7610 (2016).

[24] F. D. Natterer, K. Yang, W. Paul, P. Willke, T. Choi, T. Greber, A. J. Heinrich, and C. P. Lutz, Nature (London) 543, 226 (2017).

[25] S. Baumann, F. Donati, S. Stepanow, S. Rusponi, W. Paul, S. Gangopadhyay, I. G. Rau, G. E. Pacchioni, L. Gragnaniello, M. Pivetta, J. Dreiser, C. Piamonteze, C. P. Lutz, R. M. Macfarlane, B. A. Jones, P. Gambardella, A. J. Heinrich, and H. Brune, Phys. Rev. Lett. 115, 237202 (2015).

[26] E. Fernandes, F. Donati, F. Patthey, S. Stavrić, Z. Šljivančanin, and H. Brune, Phys. Rev. B 96, 045419 (2017).

[27] F. D. Natterer, F. Donati, F. Patthey, and H. Brune, Phys. Rev. Lett. 121, 027201 (2018).

[28] C. Piamonteze, U. Flechsig, S. Rusponi, J. Dreiser, J. Heidler, M. Schmidt, R. Wetter, M. Calvi, T. Schmidt, H. Pruchova, J. Krempasky, C. Quitmann, H. Brune, and F. Nolting, J. Synchrotron Radiat. 19, 661 (2012).

[29] K. Kummer, A. Fondacaro, E. Jimenez, E. Vélez-Fort, A. Amorese, M. Aspbury, F. Yakhou-Harris, P. van der Linden, and N. B. Brookes, J. Synchrotron Radiat. 23, 464 (2016).

[30] See Supplemental Material at http://link.aps.org/supplemental/10.1103/PhysRevLett.124.077204 for additional information on experimental and computational details, estimation of the

effective energy barrier, and models for magnetic relaxation processes.

[31] C. Wäckerlin, F. Donati, A. Singha, R. Baltic, S. Rusponi, K. Diller, F. Patthey, M. Pivetta, Y. Lan, S. Klyatskaya, M. Ruben, H. Brune, and J. Dreiser, Adv. Mater. **28**, 5195 (2016).

[32] G. H. Larson and C. D. Jeffries, Phys. Rev. **141**, 461 (1966).

[33] R. Giraud, W. Wernsdorfer, A. M. Tkachuk, D. Mailly, and B. Barbara, Phys. Rev. Lett. **87**, 057203 (2001).

[34] F. Liu, G. Velkos, D. S. Krylov, L. Spree, M. Zalibera, R. Ray, N. A. Samoylova, C.-H. Chen, M. Rosenkranz, S. Schiemenz, F. Ziegs, K. Nenkov, A. Kostanyan, T. Greber, A. U. B. Wolter, M. Richter, B. Büchner, S. M. Avdoshenko, and A. A. Popov, Nat. Commun. **10**, 571 (2019).

[35] A. Abragam and B. Bleaney, *Electron Paramagnetic Resonance of Transition Ions* (Clarendon Press, Oxford, 1970).

[36] J. Dreiser, R. Westerström, C. Piamonteze, F. Nolting, S. Rusponi, H. Brune, S. Yang, A. Popov, L. Dunsch, and T. Greber, Appl. Phys. Lett. **105**, 032411 (2014).

[37] M. Studniarek, C. Wäckerlin, A. Singha, R. Baltic, K. Diller, F. Donati, S. Rusponi, H. Brune, Y. Lan, S. Klyatskaya, M. Ruben, A. P. Seitsonen, and J. Dreiser, Adv. Sci. **6**, 1901736 (2019).

[38] N. Ishikawa, M. Sugita, T. Ishikawa, S. Koshihara, and Y. Kaizu, J. Phys. Chem. B **108**, 11265 (2004).

[39] We attribute the scattering of the data at high field to possible variations of the photon flux conditions occurring over the different experimental sessions required for the data collection.

[40] S. Roychoudhury and S. Sanvito, Phys. Rev. B **98**, 125204 (2018).

[41] D. L. Mills, Phys. Rev. **146**, 336 (1966).

[42] A more accurate computation of the relaxation rate for this process would require considering the energy and momentum dependence of the prefactor κ, which is beyond the scope of the present work.

[43] N. Ishikawa, M. Sugita, and W. Wernsdorfer, J. Am. Chem. Soc. **127**, 3650 (2005).

[44] P. R. Forrester, F. Patthey, E. Fernandes, D. P. Sblendorio, H. Brune, and F. D. Natterer, Phys. Rev. B **100**, 180405(R) (2019).

[45] Using typical values of $A_J \approx 3.5$ μeV [33,38], we estimate a hyperfine splitting $\Delta E = 2A_J \times J_z \times I \approx 170$ and 195 μeV for two possible multiplet scenarios with ground state $J_z = 7$ and 8, respectively [24].

Supplementary information
Unconventional spin relaxation involving localized vibrational modes in Ho single-atom magnets

F. Donati,[1, 2, 3] S. Rusponi,[2] S. Stepanow,[4] L. Persichetti,[4, 5] A. Singha,[1, 2, 3]
D. M. Juraschek,[4, 6] C. Wäckerlin,[2, 7] R. Baltic,[2] M. Pivetta,[2] K. Diller,[2] C. Nistor,[4]
J. Dreiser,[8] K. Kummer,[9] E. Velez-Fort,[9] N. Spaldin,[4] H. Brune,[2] and P. Gambardella[4]

[1] Center for Quantum Nanoscience, Institute for Basic Science (IBS), 03760 Seoul, Republic of Korea
[2] Institute of Physics, École Polytechnique Fédérale de Lausanne (EPFL), Station 3, CH-1015 Lausanne, Switzerland
[3] Department of Physics, Ewha Womans University, Seoul 03760, Republic of Korea
[4] Department of Materials, ETH Zurich, Hönggerbergring 64, CH-8093 Zurich, Switzerland
[5] Department of Sciences, Roma Tre University, I-00146, Roma, Italy
[6] Harvard John A. Paulson School of Engineering and Applied Sciences,
Harvard University, Cambridge, MA 02138, USA
[7] Institute of Physics of the Czech Academy of Sciences,
Cukrovarnická 10, 16200 Prague 6, Czech Republic
[8] Swiss Light Source (SLS), Paul Scherrer Institute (PSI), CH-5232 Villigen PSI, Switzerland
[9] European Synchrotron Radiation Facility (ESRF), F-38043 Grenoble, France

I. EXPERIMENTAL DETAILS

The XAS and XMCD measurements were performed at the EPFL/PSI X-Treme beamline at the Swiss Light Source [1] and at the ID32 beamline at the European Synchrotron Radiation Facility [2]. Both endstations are equipped with an ultra-high vacuum chamber for sample preparation (base pressure 3×10^{-10} mbar) and an Omicron variable-temperature scanning tunnelling microscope (VT-STM). All measurements were performed in normal incidence geometry with circularly polarized light in the total electron yield (TEY) mode at sample temperatures down to $T = 2.5$ K, and in external magnetic fields up to $B = 6.8$ T parallel to the x-ray beam. In order to isolate the contribution of the Ho atoms from the background signal, spectra of bare MgO/Ag(100) over the Ho M_5 edge are recorded prior to Ho deposition and subtracted from the final spectra.

Each point in the relaxation plot of Fig. 1 of the main text is obtained by acquiring the XAS signal for the two circular polarizations at the maximum of the XMCD edge as a function of time after saturating the ensemble to the maximum positive or negative value of the magnetic field. During the sweep of the magnetic field from the saturating to the measurement value, the beam shutter was kept close to prevent undesired photon-induced relaxation. In this way, the ensemble is largely preserved in its saturated state until the beginning of the measurement. Also note that even at high temperature we can mostly neglect spontaneous relaxation occurring prior to reach the field of measurement. In fact, these processes have been shown to be relevant only for fields below $B = 0.3$ T. The time required to sweep across this low field region and reach the target field of $B = 0.01$ T is about 10 s, a time that is not significantly relevant compared the values of τ observed in this work. Therefore, these undesired relaxation occurring prior to the measurement's start have limited impact on the experiment itself.

The XAS from the two opposite polarizations was normalized to the corresponding pre-edge signal measured 7 eV below the XMCD peak, also acquired in the same sequence, to compensate for any spurious variation of the beam intensity during the acquisition. In order to minimise the influence of the photon beam on the lifetime of the magnetic atoms [3], all the measurements were performed at the smallest photon flux ensuring a sufficient signal to noise ratio, previously shown to be $\phi_0 = 0.14 \times 10^{-2}$ nm^{-2} s^{-1} [4].

Single crystals of Ag(100) were prepared with repeated cycles of sputtering and subsequent annealing at 773 K. Films of MgO with thickness between 4 and 6 monolayers (MLs) were grown by thermal evaporation of Mg in O_2 partial pressure of 1×10^{-6} mbar, with the substrate kept at 623 K and a Mg flux yielding a growth rate of about 0.2 ML/min. One monolayer is defined as one MgO(100) unit cell per Ag(100) substrate atom. The calibration of the MgO thickness was obtained from comparison of STM images and XAS spectra at the Mg K edge of samples covered with close to half a monolayer of MgO. We then estimated the thickness of the MgO films assuming a linear relation between the amplitude of the Mg K edge and the amount of deposited MgO. The samples were transferred to the measurement position without breaking the vacuum. Holmium atoms were deposited from a thoroughly degassed rod (purity 99.95 %) on the substrate held at less than 10 K and in a base pressure of 4×10^{-11} mbar. To minimize the presence of clusters in the ensemble, we limited the Ho coverage below 0.015 ML in all the experiments, where again 1 ML is defined as one Ho atom per Ag(100) substrate atom. For the MgO thicknesses and substrate temperatures

applied here, the Ho atoms occupy with more than 90 % probability the O on-top site [5]. The amount of Ho on the surface is calibrated by comparison with former experiments [4, 6, 7].

II.   ESTIMATION OF THE EFFECTIVE ENERGY BARRIER USING ARRHENIUS FUNCTION
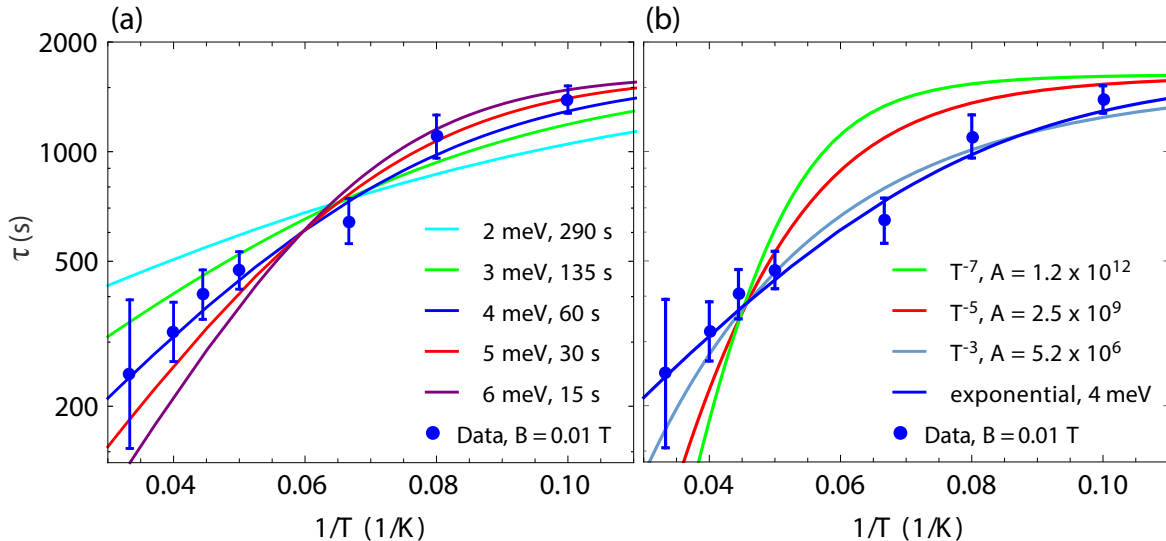
Figure S1. (a) Magnetic lifetime, τ, versus temperature for $B = 0.01$ T (blue dots). Solid lines are plots of $\tau(T)$ calculated using Eq. (S1) for different values U_{eff} and τ_0 ($\tau_\nu = 1630$ s). (b) Comparison between plots using Eq. S2 (T^{-n}) with various values of n and best fit using Eq. (S1) (exponential, blue solid line).

As discussed in the main text, the temperature dependence of τ at $B = 0.01$ T can be fit by

$$\tau_{\mathrm{Arr}}^{-1} = \tau_\nu^{-1} + \left[\tau_0 \exp\left(U_{\mathrm{eff}}/k_{\mathrm{B}}T\right)\right]^{-1}, \tag{S1}$$

where $\tau_\nu = 1630$ s is the photon-limited lifetime due to the secondary electrons [4], and the exponential term describes a thermally-activated relaxation with an effective barrier U_{eff} and a prefactor τ_0. As shown in Fig. S1(a), best fit to the data gives $U_{\mathrm{eff}} = 4 \pm 1$ meV and $\tau_0 = 60 \pm 30$ s.

In order to further evince the origin of this relaxation process, we consider the expected rate obtained from Raman-processes activated by the continuum of delocalized substrate phonons. In this case, one finds a relaxation rate that follows a power law [8, 9] with characteristic exponent depending on the spin multiplicity and dimensionality of the phonon modes. Including the photon-limited relaxation, the magnetic lifetime reads

$$\tau_{Ram}(T)^{-1} = \tau_\nu^{-1} + \left[AT^{-n}\right]^{-1}, \tag{S2}$$

with A being a rescaling prefactor. For non-Kramers ions, the characteristic exponent takes values of $n = 7$ or 5 when phonon modes with 3D or 2D dispersion relations, respectively, are involved. Best fits using these two power laws cannot reproduce the low field data, see Fig. S1(b). Only lowering the exponent to $n = 3$ produces a fair fit, although less accurate than the best fit using Eq. (S1).

The required low value of the characteristic exponent suggests that the coupling to delocalized phonons cannot account for the observed spin relaxation. In the literature, non-conventional values of the characteristic exponent are often found in molecules with very large magnetic anistropy [10, 11] and attributed to the presence of localized modes with sharp resonances in the DOS. As shown in Sec. IV, a proper description of these local modes in surface-adsorbed atoms leads to a characteristic exponential temperature law. We finally note that, even if a power law with low exponent could provide an approximate fit to the low field data, processes that involves a monotonic phonon DOS are expected to provide a relaxation rate that increases with the external field, see Sec. IV, hence they cannot account for the observed behavior at high field.
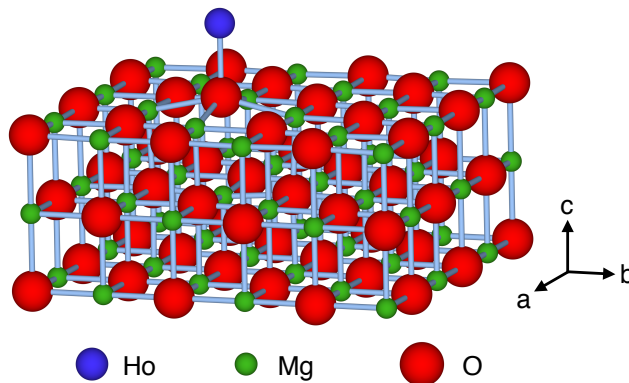
Figure S2. Unit cell of one Ho atom on three monolayers of MgO with the bottom layer fixed to the lattice spacing of Ag(100) at 289 pm. The oxygen lying below the Ho is protruded from the surface by 47±2 pm.

III. COMPUTATIONAL DETAILS

We calculated the vibrational eigenfrequencies and eigenvectors of a Ho atom on three monolayers of MgO from first-principles using the density functional theory (DFT) formalism as implemented in the Vienna ab-initio simulation package (VASP) [12, 13] and the frozen-phonon method as implemented in the phonopy package [14]. We used a 109-atom unit cell with Ho located above a surface oxygen and topped by 16 Å of vacuum, and we fixed the bottom MgO layer to the lattice spacing of Ag(100) at 289 pm. Since MgO was shown to act as an efficient filter for the phonon modes of a substrate [4], we do not take the Ag substrate into account in this calculation. We used the default VASP PAW pseudopotentials and converged the Hellmann-Feynman forces to 10^{-5} eV/Å using a plane-wave energy cut-off of 750 eV and a $2 \times 2 \times 1$ k-point mesh to sample the Brillouin zone. For the exchange-correlation functional we chose the PBEsol form of the generalized gradient approximation (GGA) [15, 16]. Our fully relaxed structure with a MgO surface lattice spacing of 289 pm fits reasonably well to the experimental values [4]. The Ho atom is elevated 251±1 pm above the slightly buckled MgO surface and 204 pm above the protruded oxygen. An illustration of the unit cell is shown in Fig. S2. Crystal structures were visualized using the VESTA package [17].
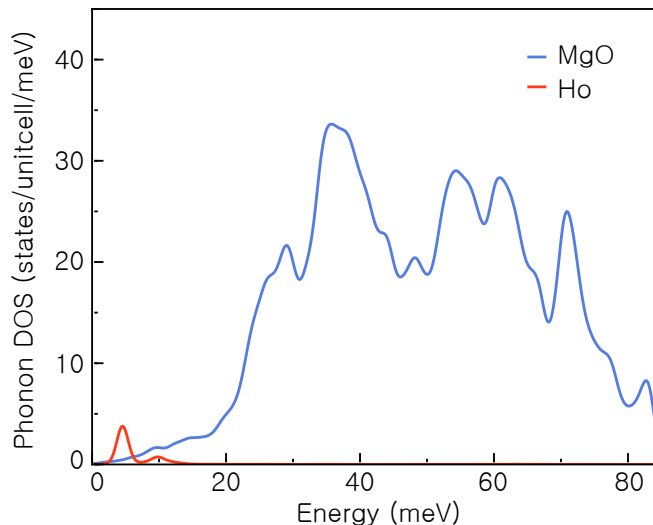
Figure S3. Calculated phonon DOS projected onto the contributions of the Ho atom and the MgO slab, respectively.

Frozen-phonon calculations reveal two degenerate modes at the Brillouin zone center involving mainly the motion of the Ho atom parallel to the surface at 4.7 meV and perpendicular to the surface at 8.6 meV. These vibrations distinctively show up in the phonon density of states as two peaks in the low-frequency regime, as is shown in Fig. 4a of the main text and in Fig. S3. Vibrational modes involving mainly the ions of the MgO slab lie at higher frequencies above roughly 20 meV. The eigenvectors of the Ho atom and the below lying oxygen are shown schematically in

Fig. 4b of the main text. Our calculation of the localized vibrational modes yields two degenerate in-plane modes and one out-of-plane mode in accordance with the P4mm symmetry of the Ho adsorption site on top of oxygen, and in contrast to previous calculations, in which the symmetry was not maintained [4].

The calculated phonon DOS supports the assumptions of the two-phonon relaxation model developed in this work, with the local vibrations providing the largest contribution. The main arguments supporting the weak coupling to the MgO delocalized phonon modes are the following. Firstly, at low energy the phonon DOS of the acoustic modes is quite low. In addition, the long range waves only provide very small relative displacement on the atomic scale, which in turns limits the effect on the local change of the magnetic anisotropy. Secondly, although optical phonon modes could provide the required perturbation to the local environment [18], the high energy required to activate these modes in MgO $(50 - 80 \text{ meV})$ strongly limits their contribution in the temperature range of our experiments. Consequently, the most effective contribution to the spin-reversal has to stem from the local vibrations, as these modes provide large displacement of the Ho atoms at an energy that can be activated at low temperature, as shown in Fig. S3.

IV. RAMAN MODEL OF MAGNETIC RELAXATION

The long magnetic lifetimes measured at low fields and the large magnetic remanence observed in hysteresis loops [4] suggests that, for Ho atoms, quantum tunneling of the magnetization is slower than the photon-induced relaxation. Similarly, the absence of a characteristic decrease of the spin lifetime with increasing magnetic field suggests that direct processes are not effectively contributing to the spin relaxation up to the longest time scale available in our experiments (thousands of seconds). As discussed in a previous work [19], two alternative level schemes with either $J_z = 7$ or 8 ground state can possibly explain the available experimental data [4, 19, 20]. In a more recent paper [21], it was shown that the behavior of Ho atoms at small magnetic fields is compatible with a $J_z = 8$ ground state where the hyperfine interaction creates several avoided level crossings. In both scenarios, due to the C_{4v} symmetry of the adsorption site, the ground state doublet is not a pure state of the operator $\hat{J}_z$ and the admixture of states with lower axial character enables transitions across the anisotropy barrier. Assuming the eigenstates of the system to be product states between spin and phonon states [22], spin reversal can occur through $\Delta m = \pm 2$ or $\Delta m = 0$ transitions for a $J_z = 7$ or 8 ground state, respectively. In both cases, realizing these transitions requires the transfer of angular momentum of two quanta carrying a momentum $\Delta m = \pm 1$ [22]. Supported by these arguments, and in the absence of clear signatures related to spin reversal driven by quantum tunnelling of the magnetization and direct processes, we develop a model for the magnetic lifetime of Ho atoms that only includes two-phonon Raman processes and photon-induced relaxation.

Specifically, we include the contribution of spatially localized vibrations following the approach of D.L. Mills [23]. These vibrational modes are modeled with gaussian peaks:

$$D_v(\omega - \omega_v) = \frac{\exp\left[\frac{(\omega - \omega_v)^2}{2\sigma_\omega^2}\right]}{\hbar\sqrt{2\pi}\sigma_\omega} \tag{S3}$$

at the frequencies $\omega_v = \omega_\parallel = E_\parallel/\hbar = 4.7 \text{ meV}/\hbar$ and $\omega_v = \omega_\perp = E_\perp/\hbar = 8.6 \text{ meV}/\hbar$ as calculated by DFT. The broadening σ_ω is related to the full-width-half-maximum (FWHM) of the gaussian peak by $\Delta\omega = \Delta E/\hbar = 2\sqrt{2\ln 2}\sigma_\omega$. It is a free parameter of the model and is determined from the fit of the experimental data. For the model described in the main text, we only include the projected phonon DOS on the Ho atoms:

$$D_{\text{Ho}}(\omega) = 2D_v(\omega - \omega_\parallel) + 0.4D_v(\omega - \omega_\perp), \tag{S4}$$

where the factor of 2 for the $D_v(\omega - \omega_\parallel)$ accounts for the two-fold degeneracy of the in-plane vibrational mode. As shown in Fig. 4 b of the main text, the Ho out-of plane mode involves the motion of the oxygen atom underneath it, hence part of its amplitude is projected on the MgO phonon DOS. To account for this effect, in $D_v(\omega - \omega_\perp)$ we rescaled the peak amplitude to 0.4 to reproduce the relative heights of the phonon DOS peaks projected only on the Ho atoms, as calculated with DFT (see Fig. 4a of the main text). We then compute the related phonon energy density:

$$\rho_{\text{Ho}}(\omega, T) = D_{\text{Ho}}(\omega)\langle\hbar\omega\rangle = D_{\text{Ho}}(\omega)\left[\exp\left(\frac{\hbar\omega}{k_B T}\right) - 1\right]^{-1} \tag{S5}$$

to evaluate the transition probability obtained from the two-phonon integral [8, 23]

$$\Gamma(B, T) = \kappa \int_0^{\omega_c} \rho_{\text{Ho}}(\omega, T)\rho_{\text{Ho}}\left(\omega + \frac{\Delta}{\hbar}, T\right)\exp\frac{\hbar\omega + \Delta}{k_B T}d\omega. \tag{S6}$$

Here, ω and $\omega + \frac{\Delta}{\hbar}$ are the frequencies of the two phonons involved in the transition, with $\Delta = 2\mu_{\text{Ho}}B$ being the Zeeman splitting between the two lowest states with $\mu_{\text{Ho}} = 10.1\,\mu_{\text{B}}$ [20]. We set the cut-off frequency of the integration $\omega_c = E_c/\hbar = 100$ meV/$\hbar$ while κ is an overall scaling factor that depends on the properties of the materials and on the spin-phonon coupling [8]. Due to the peculiar single-bond-coordination of Ho atoms on MgO, most of the physical quantities used to determine this factor, such as the velocity of sound and material density, do not have a proper definition for the present system. Assuming a constant energy and momentum dependence of the spin-phonon coupling for the sake simplicity, the value of κ is, therefore, a constant, which is taken as a free parameter of the model. A more complete approach to compute the relaxation rate of single atom magnets by properly summing over all the momentum-dependent relaxation paths is beyond the scope of the present analysis and will be addressed in a future work.

The terms $\rho(\omega, T)$ and $\rho(\omega + \Delta/\hbar, T)\exp\frac{\hbar\omega+\Delta}{k_{\text{B}}T}$ describe the absorption and emission of a phonon, respectively, connecting the two states separated by an energy $\Delta = 2\mu_{\text{Ho}}B$, with $\mu_{\text{Ho}} = 10.1\mu_{\text{B}}$ [20]. The magnetic lifetime is obtained including the rates of the two possible reversal events ($|+\rangle$ to $|-\rangle$ and back) from the inverse sum of the respective rates, which can be expressed by [23]:

$$\tau_{\text{s}}(B,T)^{-1} = \Gamma(B,T)\left[1 + \exp\frac{-\Delta}{k_{\text{B}}T}\right]. \tag{S7}$$

Finally, the experimental lifetime is modeled by inversely adding the photon-limited lifetime τ_ν from the cascade of secondary electrons generated in the x-ray absorption process to the spin reversal lifetime:

$$\tau(B,T)^{-1} = \tau_\nu^{-1} + \tau_s(B,T)^{-1}, \tag{S8}$$

with the values of τ_ν taken from previous flux-dependent lifetime measurements [4]. In agreement with the analytical derivation presented in the work from D. L. Mills et al., the presence of a sharp resonance in the phonon DOS produces an exponential term in the temperature behavior of the spin relaxation [23]. As seen from the full curves in Figs. 2 and 3 of main text, our model reproduces the temperature- and field-dependent data for $\kappa = 1.7 \times 10^{-17}$, $\Delta E = 0.17$ meV.

To verify the potential role of delocalized MgO phonons to the reversal of Ho spins, we produce comparative models that include 2D delocalized phonons either in the absence or in the presence of local vibrational modes in the effective total DOS. According to our DFT calculations, the low-energy part of the MgO phonon DOS shows an almost linear increase with energy (see Fig. 4 of main text and first part of the blue curve of Fig. S3 above). Therefore, we firstly model the delocalized MgO phonons by a linear density of states:

$$D_{\text{MgO}}(\omega) = \beta\hbar\omega, \tag{S9}$$

with a slope $\beta = 0.066$ meV^{-2} matching the DOS of Fig. 4a of the main text, and use the corresponding phonon energy density $\rho_{\text{2D}}(\omega, T) = D_{\text{2D}}(\omega)\langle\hbar\omega\rangle$ to compute the magnetic lifetime. Figure S4(a) shows the calculated temperature dependence of τ for low and high fields. The low field curve from our model follows closely the T^{-5} power law expected for Raman relaxation from phonons with 2D dispersion. Instead, the high field curve does not follow the same functional dependence and the calculated magnetic lifetimes are always lower than the corresponding low field values. This effects is generally valid for every monotonic phonon DOS and stems from the increased availability of phonons state for emission when larger splitting of the states are involved [8]. Figure S4(b) shows the comparison between experiments and calculated lifetime including the Raman process from delocalized phonon modes only and photon-induced relaxation background. As also discussed in Sec. II, this model provides a poor fit at low field and cannot capture at all the experimental behavior at high field.

We additionally test a comparative model that includes both delocalized and local vibrational modes. In this case, the total phonon density of states

$$D_{\text{tot}}(\omega) = D_{\text{MgO}}(\omega) + 2D_{\text{v}}(\omega - \omega_\parallel) + D_{\text{v}}(\omega - \omega_\perp) \tag{S10}$$

is computed by summing the amplitudes of all Ho- and MgO-projected components of the respective phonon DOS. Therefore, the total DOS at the in-plane and out-of-plane modes energy must follow the related degeneracy, namely 2 and 1, respectively. For this reason, we omit the rescaling factor of 0.4 for the out-of-plane peak at 8.6 meV (see Fig. 4a of the main text). We again use the phonon energy density $\rho_{\text{tot}}(\omega, T) = D_{\text{tot}}(\omega)\langle\hbar\omega\rangle$ to compute the magnetic lifetime as described above.

Figure S5 shows the result of the fit of temperature-dependent data with the relaxation model obtained using D_{tot} from Eq. S10, $\kappa = 1.0 \times 10^{-17}$, $\Delta E = 0.17$ meV. Although the low field data in Fig. S5a and low temperature data in Fig. S5b are quite well reproduced, the lifetime at high-field and high temperature cannot be captured by this model. This discrepancy is due to the overestimation of the coupling term between the spin and the delocalized phonon DOS. As the phonon DOS increases with the energy of the mode (see Eq. S9), more phonons are available to match the
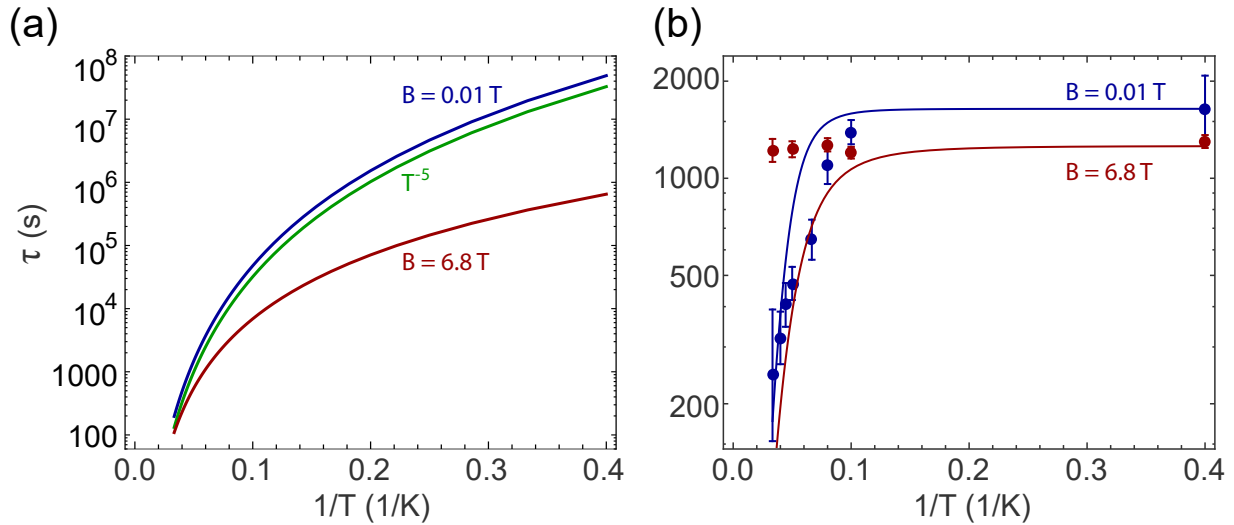
Figure S4. (a) Calculated magnetic lifetime, τ, for a two-phonon Raman process activated by delocalized MgO phonons with 2D dispersion (Eq. S9). Values obtained for $B = 0.01$ T (blue) and $B = 6.8$ T (red) are compared to a AT^{-5} power law (green) ($\kappa = 1.2 \times 10^{-16}$, $\mu_{\text{Ho}} = 10.1\mu_{\text{B}}$, $A = 3.5 \times 10^{9}$ sK^{-5}). (b) Magnetic lifetime, τ, as a function of temperature for $B = 0.01$ T (blue) and $B = 6.8$ T (red). Calculated magnetic relaxation τ including two-phonon Raman process with MgO phonons and photon-induced relaxation background (solid lines) are compared with experimental data (dots).

transition energies when the spin states are split in an external magnetic field. As a consequence, the contribution of the substrate phonons to the integral in Eq. (S6) increases with increasing values of $\Delta \propto B$. Using the model that only includes local displacements on the Ho atoms, the fits to high- field and high-temperature data are notably improved as shown in the main text in Fig. 2. These results suggest that the mechanism for Ho spin relaxation is predominantly the coupling with the local vibrational modes, as also proposed for molecular magnets [24]. As these modes induce a large Ho displacement with respect to the MgO lattice, they generate large low-symmetry distortions of the C_{4v} static crystal field of the oxygen top adsorption [4, 5], providing an efficient pathway to the spin relaxation [8].

Finally, we note that the localized vibrations provide significant contribution only to the two-phonon Raman processes, while no signature of direct process relaxation has been detected, i.e., at fields for which the Zeeman splitting matches the energy of the local modes (4.1 T and 7.4 T for the in-plane and out-of-plane mode, respectively).
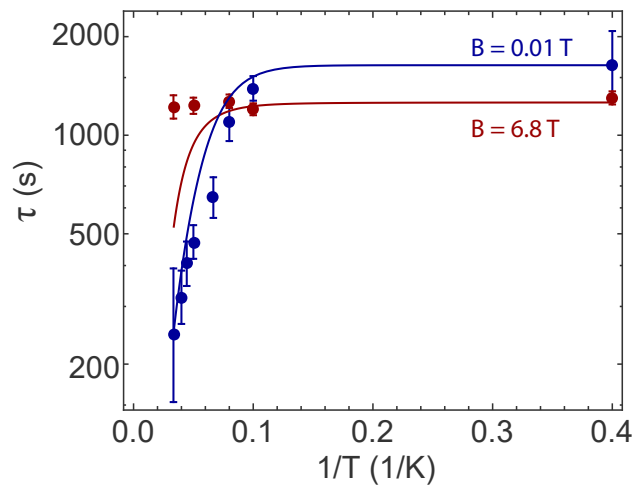
Figure S5. Magnetic lifetime, τ, as a function of temperature for $B = 0.01$ T (blue) and $B = 6.8$ T (red). Two-phonon Raman process including both Ho localized vibrations and delocalized MgO phonons contribution are shown as full lines ($\kappa = 1.0 \times 10^{-17}$, $\Delta E = 0.17$ meV, $\hbar\omega_{\parallel} = 4.7$ meV, $\hbar\omega_{\perp} = 8.6$ meV $\mu_{\text{Ho}} = 10.1\mu_{\text{B}}$) in comparison with experimental data shown as dots.

This suggests that the corresponding matrix element for transition of direct processes is significantly smaller than that of the Raman process.

V. ORBACH MODEL OF MAGNETIC RELAXATION

We test the validity of our conclusion by comparing these results with those obtained from a relaxation model that assumes only delocalized MgO phonons with 2D dispersion and a singlet excited state at $\overline{E} = \hbar\overline{\omega} = 4.5$ meV, as inferred from previous multiplet calculations [4]. In this case, an Orbach process with activation barrier $\overline{E}$ is expected to give a characteristic lifetime with an exponential temperature behavior, even in the absence of a localized mode [8]. The magnetization reversal rate for a two-phonon Orbach process is:

$$\overline{\Gamma}_{-J_z \to +J_z}(B,T) = \kappa^* \rho_{MgO}(\overline{\omega} - \frac{\Delta}{2\hbar}, T)\rho_{MgO}(\overline{\omega} + \frac{\Delta}{2\hbar}, T) \exp\frac{\hbar\overline{\omega} + \Delta/2}{k_B T},$$

(S11)

with

$$\rho_{MgO}(\omega, T) = D_{MgO}(\omega)\frac{\hbar\omega}{\exp\frac{\hbar\omega}{k_B T} - 1}$$

(S12)

being the energy density of the MgO phonons only. Similarly to our analysis of the Raman process, we fit the experimental data by considering reversal from both J_z states and including the effect of the x-ray induced secondary electrons, as described in Eqs. (S7) and (S8). The results of the model for the temperature-dependent data at fixed field are shown in Fig. S6 for $\kappa^* = 5.0 \times 10^{-3}$ s^{-1}. Again, the low-field behavior is quite well reproduced, however, the model fails at high field. This failure is due to the decreasing separation between one of the Zeeman-split states of the lowest doublet and the excited-state singlet with increasing field, which produces a reduction of the energy barrier for reversal. The comparison between data and model indicates that long magnetic lifetimes at high magnetic field are not compatible with the presence of a first excited-state singlet at low energy. The presence of this singlet state, although predicted by multiplet calculations, has so far not been found in STM experiments [19, 20]. Our results further support the level schemes such as those discussed in Ref. [19] for explaining the magnetic states of Ho atoms.
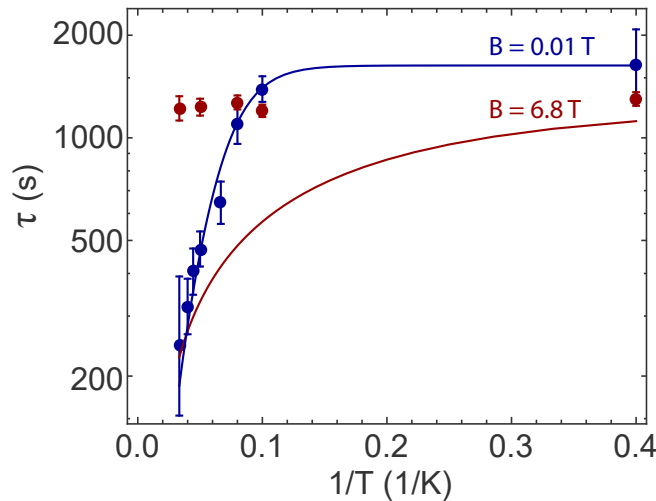
Figure S6. Magnetic lifetime, τ, as a function of temperature for $B = 0.01$ T (blue) and $B = 6.8$ T (red). Calculated τ including photon-induced relaxation background and a two-phonon Orbach process activated by delocalized MgO phonons with 2D dispersion (solid lines) are compared with experimental data (dots) ($\kappa^* = 200$, $\mu_{Ho} = 10.1\mu_B$, $\hbar\overline{\omega} = 4.5$ meV) in comparison with experiment shown as dots.

[1] C. Piamonteze, U. Flechsig, S. Rusponi, J. Dreiser, J. Heidler, M. Schmidt, R. Wetter, M. Calvi, T. Schmidt, H. Pruchova, J. Krempasky, C. Quitmann, H. Brune, and F. Nolting, J. Synchr. Rad. 19, 661 (2012).

[2] K. Kummer, A. Fondacaro, E. Jimenez, E. Vélez-Fort, A. Amorese, M. Aspbury, F. Yakhou-Harris, P. van der Linden, and N. B. Brookes, J. Synchr. Rad. **23**, 464 (2016).

[3] J. Dreiser, R. Westerström, C. Piamonteze, F. Nolting, S. Rusponi, H. Brune, S. Yang, A. Popov, L. Dunsch, and T. Greber, Appl. Phys. Lett. **105**, 032411 (2014).

[4] F. Donati, S. Rusponi, S. Stepanow, C. Wäckerlin, A. Singha, L. Persichetti, R. Baltic, K. Diller, F. Patthey, E. Fernandes, J. Dreiser, Ž. Šljivančanin, K. Kummer, C. Nistor, P. Gambardella, and H. Brune, Science **352**, 318 (2016).

[5] E. Fernandes, F. Donati, F. m. c. Patthey, S. Stavrić, i. c. v. Šljivančanin, and H. Brune, Phys. Rev. B **96**, 045419 (2017).

[6] F. Donati, A. Singha, S. Stepanow, C. Wäckerlin, J. Dreiser, P. Gambardella, S. Rusponi, and H. Brune, Phys. Rev. Lett. **113**, 237201 (2014).

[7] A. Singha, F. Donati, C. Wäckerlin, R. Baltic, J. Dreiser, M. Pivetta, S. Rusponi, and H. Brune, Nano Lett. **16**, 3475 (2016).

[8] A. Abragam and B. Bleaney, *Electron paramagnetic resonance of transition ions* (Clarendon Press, Oxford, 1970).

[9] L. T. A. Ho and L. F. Chibotaru, Phys. Rev. B **97**, 024427 (2018).

[10] C. A. P. Goodwin, F. Ortu, D. Reta, N. F. Chilton, and D. P. Mills, Nature **548**, 439 (2017).

[11] F.-S. Guo, B. M. Day, Y.-C. Chen, M.-L. Tong, A. Mansikkamaki, and R. A. Layfield, Science **362**, 1400 (2018).

[12] G. Kresse and J. Furthmüller, Comput. Mat. Sci. **6**, 15 (1996).

[13] G. Kresse and J. Furthmüller, Phys. Rev. B **54**, 11169 (1996).

[14] A. Togo and I. Tanaka, Scr. Mater. **108**, 1 (2015).

[15] J. Perdew, A. Ruzsinszky, G. Csonka, O. Vydrov, G. Scuseria, L. Constantin, X. Zhou, and K. Burke, Phys. Rev. Lett. **100**, 136406 (2008).

[16] G. I. Csonka, J. P. Perdew, A. Ruzsinszky, P. H. T. Philipsen, S. Lebègue, J. Paier, O. A. Vydrov, and J. G. Ángyán, Phys. Rev. B **79**, 155107 (2009).

[17] K. Momma and F. Izumi, J. Appl. Crystallogr. **44**, 1272 (2011).

[18] L. Escalera-Moreno, J. J. Baldoví, A. Gaita-Ariño, and E. Coronado, Chem. Sci. **9**, 3265 (2018).

[19] F. D. Natterer, F. Donati, F. Patthey, and H. Brune, Phys. Rev. Lett. **121**, 027201 (2018).

[20] F. D. Natterer, K. Yang, W. Paul, P. Willke, T. Choi, T. Greber, A. J. Heinrich, and C. P. Lutz, Nature **543**, 226 (2017).

[21] P. R. Forrester, F. m. c. Patthey, E. Fernandes, D. P. Sblendorio, H. Brune, and F. D. Natterer, Phys. Rev. B **100**, 180405 (2019).

[22] C. Calero, E. M. Chudnovsky, and D. A. Garanin, Phys. Rev. B **74**, 094428 (2006).

[23] D. L. Mills, Phys. Rev. **146**, 336 (1966).

[24] S. Roychoudhury and S. Sanvito, Phys. Rev. B **98**, 125204 (2018).